HAL open science

Mesh regularization of ablating hypersonic vehicles

Claire Roche, Jerome Breil, Marina Olazabal

To cite this version:

Claire Roche, Jerome Breil, Marina Olazabal. Mesh regularization of ablating hypersonic vehicles. 8th European Congress on Computational Methods in Applied Sciences and Engineering (ECCOMAS 2022), Jun 2022, Oslo, Norway. cea-03783795

HAL Id: cea-03783795

https://cea.hal.science/cea-03783795v1

Submitted on 22 Sep 2022

HAL is a multi-disciplinary open access archive for the deposit and dissemination of scientific research documents, whether they are published or not. The documents may come from teaching and research institutions in France or abroad, or from public or private research centers.

L'archive ouverte pluridisciplinaire **HAL**, est destinée au dépôt et à la diffusion de documents scientifiques de niveau recherche, publiés ou non, émanant des établissements d'enseignement et de recherche français ou étrangers, des laboratoires publics ou privés.

The 8th European Congress on Computational Methods in Applied Sciences and Engineering
ECCOMAS Congress 2022
5-9 June 2022, Oslo, Norway

MESH REGULARIZATION OF ABLATING HYPERSONIC VEHICLES

CLAIRE ROCHE[1], JEROME BREIL[1] and MARINA OLAZABAL[1]

[1] CEA CESTA, 16 Av. des Sablieres, 33114 Le Barp
email: claire.roche@cea.fr

Key words: Mesh regularization, Mesh refinement, Mesh movement, Hypersonic

Abstract.

The ablation of a vehicle during atmospheric reentry leads to a degradation of its surface state. Ablated wall interacts with the boundary layer that develops around the object. The deformation can be seen as a ripple or a roughness pattern with different characteristic amplitudes and wavelengths. The effect on the flow is taken into account either by means of modelizations or by direct simulation by applying the deformation to the mesh.

Mesh regularization techniques can be used in order to take into account wall deformations during a simulation. In this work we apply our regularization directly to a mesh which has been already deformed. The meshes will be adapted for use in a parallel CFD Navier-Stokes code. A refinement of the mesh close to the wall is required to correctly capture the boundary layer, but also to accuratly represent the geometry of the wall deformation. For the numerical methods used, a constraint of orthogonality is added to the mesh impining on the wall.

1 INTRODUCTION

The ablation of a vehicle during an atmospheric re-entry leads to a degradation of its surface state. This degraded wall interacts with the laminar flow and then turbulent boundary layer develops around the object. The deformation can be likened to a ripple or roughness pattern with different characteristic amplitudes and wavelengths. The effect on the flow can be taken into account through modelling. Here, the deformation of the wall will be taken into account by applying deformation of the wall directly to the mesh.

In the field of hypersonic reentry due to the physics (boundary layer, shock, etc...) and numerical methods used in the computer code we often need to work with structured meshes. In order to take into account the wall deformations during the calculation it is necessary to work with regularization methods that can be applied to this type of mesh [6]. There is therefore a need for methods that are both efficient and robust in order to create or adapt a mesh for this phenomenon.

When a geometry with a deformation or a change in slope is considered, the mesh must be refined around these asperities in order to properly represent the geometry of the wall. In addition, several physical phenomena appear in the simulations where the Navier-Stokes equations are solved, the development of a boundary layer in the near wall region, but also shock waves, expansion waves or recirculation zones. It is preferable to refine the mesh in these zones in order to capture the phenomena due to the appearance of strong gradients. An

additional constraint resides in the conservation of the orthogonality of the cells to the wall in order to align the cells with the flow.

In summary, as the physics in the boundary layer is the main interest in this study, it is chosen to impose an orthogonality of the mesh on the wall, as well as a refinement of the mesh on the wall and around the deformations. The code for solving the Navier-Stokes and Euler equations used in this study imposes working with structured meshes. Moreover, the nodes placed on the wall are fixed during the calculation, while the sliding of the nodes on the outer fluid boundaries is allowed.

The first part of this paper is devoted to the presentation of the mesh regularization used in this study. The Line-Sweeping method [6] has been implemented in order to regularize deformed meshes. This method was then adapted to take into account the constraint of orthogonality of the meshes to the wall for the geometries treated. Then, progression law for the refinement of the near-wall mesh, the β law, is presented. The goal is to impose the size of the first cell of the mesh in order to capture the dynamics of the flow in the boundary layer during the simulation. Finally, simulations of flows in hypersonic regime along a flat plate with wall deformations using the Navier-Stokes CFD code are performed. A final simulation on a Cone-Cylinder-Flare configuration is presented in order to test the regularization method on realistic geometries.

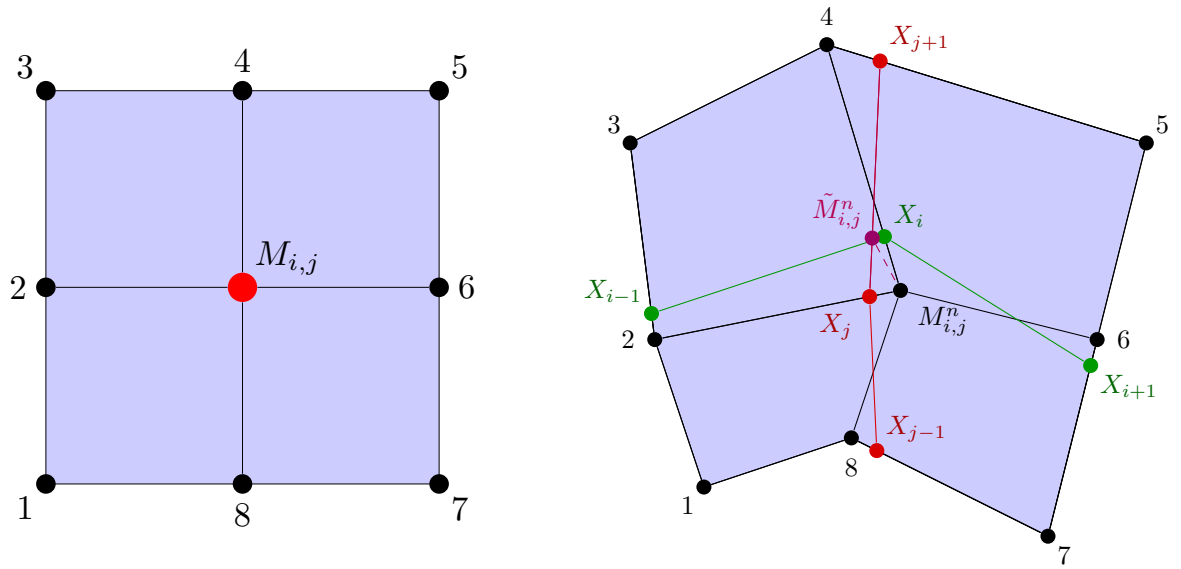

(a) Node to be moved in red, stencil for the Line-Sweeping method in black.

(b) Line-Sweeping regularization method in 2D.

Figure 1: Presentation of the Line-Sweeping regularization method in 2D with the stencil in order to move a node.

2 REGULARIZATION, ADAPTATION AND REFINEMENT OF THE MESH

2.1 Line-Sweeping regularization method

The Line-Sweeping method presented by Jin Yao [7] is a local iterative geometric method allowing to regularize a structured mesh in order to smooth the mesh in a uniform way. The goal is to replace each node according to the position of its neighbors until convergence of the regularization or until obtaining a solution considered acceptable.

The stencil of the method for moving a node is shown in Figure 1.(a), the red node being the one that needs to be repositioned. In Figure 1.(b), the Line-Sweeping method is shown in 2D. The black nodes correspond to the mesh at iteration n. Six fictitious points are calculated, point X_{i-1} is placed in the middle of the branch of points 1 to 3, the other green points are also placed in the middle of the vertical branches. Red nodes like X_{j+1} are placed in the middle of the horizontal branches. The calculated point, $\tilde{M}^n_{i,j}$ is at the intersection of the red and green branches formed by the points X_i, X_j. Finally, the damping parameter θ allows to place the new node $M^{n+1}_{i,j}$ according to the equation (1). Here, the node will be on the segment $[\tilde{M}^n_{i,j}; M^n_{i,j}]$ depending on the value of θ.

$$M^{n+1}_i = \theta M^n_{i,j} + (1-\theta)\tilde{M}^n_{i,j} \tag{1}$$

In the case of non-uniform mesh on the wall we use weights in order to propagate non-uniform distribution of the nodes on the wall. The weights are such that they respect the ratio between the nodes on the wall and using another damping parameter, we will have a uniform mesh far from the wall.

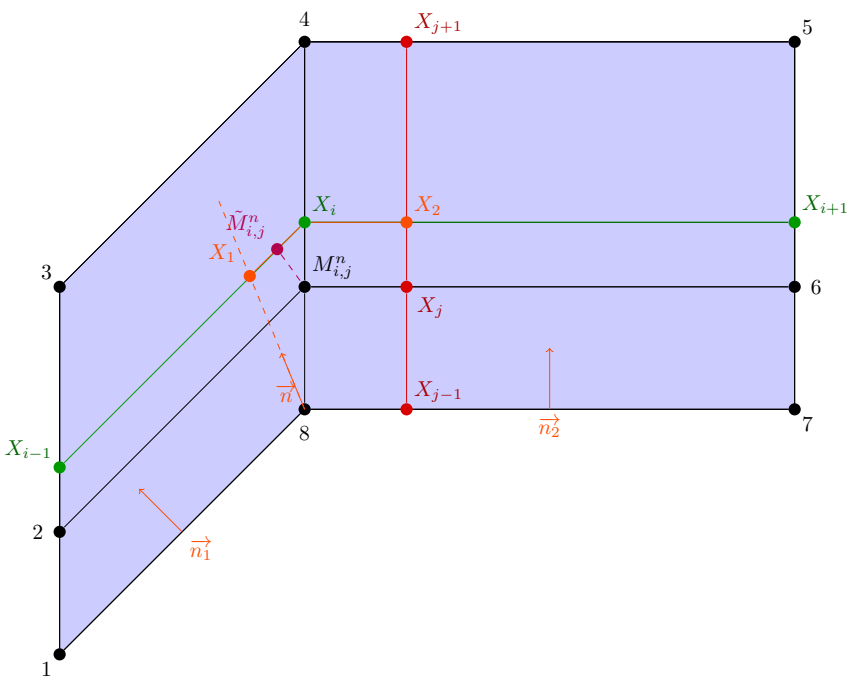

Figure 2: Line-Sweeping method with orthogonality criterion in 2D.

2.2 Line-Sweeping method adapted to the orthogonality constraint

In order to impose the orthogonality of the meshes on the wall, the Line-Sweeping method was modified such that we can get orthogonal mesh on the wall. To move a node, the stencil is the same as for the Line-Sweeping 2D method shown in Figure 1.(a). To find the new position of the node, two points are calculated, denoted X_1 and X_2 in Figure 2. The point X_2 is placed by the Line-Sweeping 2D method. To find the position of point X_1, the normals $\overrightarrow{n_1}$ and $\overrightarrow{n_2}$ are calculated relative to the segments of the wall as shown in the diagram, then the sum of these two vectors $\overrightarrow{n}$ is chosen to evaluate the point X_1. The point X_1 is then the intersection between the line carried by the vector $\overrightarrow{n}$ passing through the node $n°8$, and the branch of the X_i represented in green. These two points make it possible to define a new branch in orange and contained on the green branch. Finally, a coefficient $\alpha \in [0, 1]$ controls whether the new node will be closer to point X_1 or point X_2, but still on the orange branch. An example of the calculation of the coefficient α will be illustrated in the part presenting the results obtained using this method of regularization (2.3). For the calculation of the coefficient α, parameters related to the shape of the wall can be taken into account. In the context of this study, it is calculated according to the height of the node in the y direction and allows the constraint of orthogonality to the wall to be relaxed as the nodes is far from it. In Figure 2 the orthogonalization is done with respect to the adjacent mesh line.

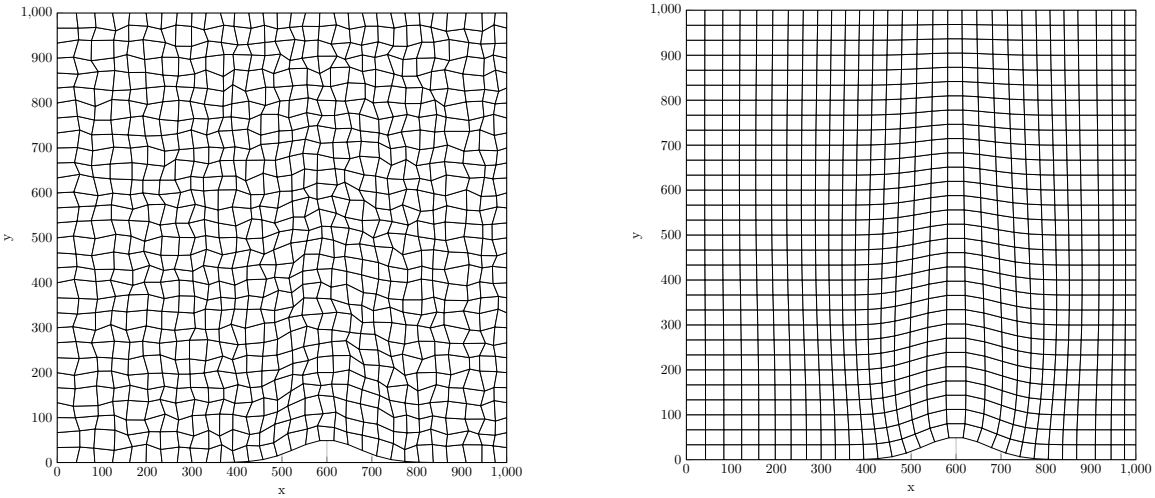

(a) Initial degraded mesh of a flat plate with a bump of size 30×30 with a non-uniform distribution of nodes on the wall.

(b) Mesh 30×30 obtained after 1000 iterations of the Line-Sweeping regularization taking into account the weights and orthogonalization of the meshes to the wall

Figure 3: Line-Sweeping regularization with consideration of weights relative to the distribution of nodes on the wall with orthogonalization of meshes near wall on a mesh of size 30×30.

2.3 2D Line-Sweeping method taking into account the orthogonality criterion

As shown previously the Line-Sweeping method has been modified in order to take into account the orthogonality criterion of the cells to the wall. The choice of an increasing function with values in the interval $[0, 1]$ for the calculation of the coefficient α along the lines of mesh makes it possible to impose a more or less strong orthogonality in the mesh. For the regularization presented in Figure 3, we choose $\alpha = (\frac{j-1}{N_y})^{0.1}$ where j is the index of the node according to the direction y, and N_y the number of cells in this same direction. Starting from the mesh randomly perturbed of Figure 3.(a), 1000 iterations of the Line-Sweeping method taking into account the weights and the orthogonalization criterion are carried out, with a damping coefficient $\theta = 0.2$. This regularization makes it possible both to obtain orthogonal meshes at the level of the wall, but also to release this constraint quite gently so that there is no sudden jump in the mesh sizes in the domain.

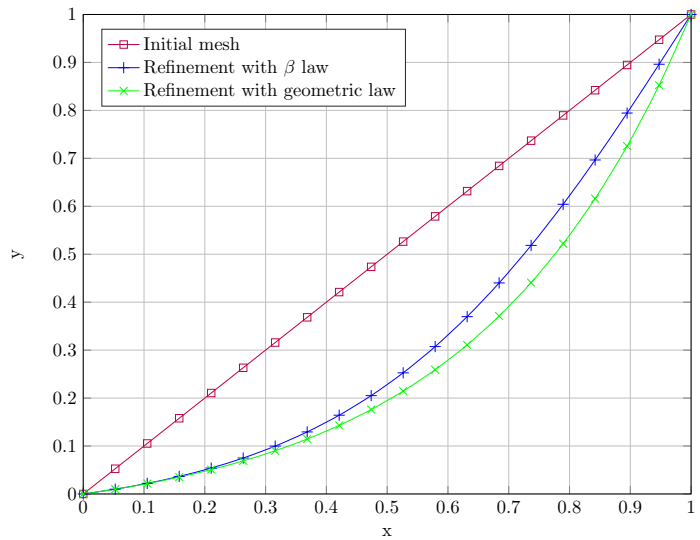

Figure 4: Comparison of the refinement of a 1D mesh by the Beta law and by the geometric law for a first mesh size imposed at 10^{-2}.

2.4 Refinement β law

The β law is a refinement law with an exponential function. This refinement law is often used in boundary layer simulation as it allows to have a very small cell close to the wall and few cells far from it. This can be used in a context of structured meshes to obtain a refinement of the meshes around the boundary layer. To apply this law on a 1D mesh, we simply iterate over the nodes concerned as follows:

$$x_i = x_1 + f_n(x_{N_x+1} - x_1) \tag{2}$$

with

$$f_n = 1 + \beta \frac{1 - e^p}{1 + e^p} \tag{3}$$

where $p = z(1-n)$, $z = log(r)$, $r = \frac{\beta+1}{\beta-1}$ and $n = \frac{i-1}{N_x}$.
Here N_x is the number of cells and x_i is the i-th node of the mesh for $i \in 1, ..., N_x + 1$. $\beta \in [1.00001, 1.01]$ acts as an expansion coefficient. For low value of β, the mesh will be refined on the wall. The points x_1 and x_{N_x+1} at the edge of the domain are fixed.

Using a Newton it is possible to impose the size of the first cell and find the associated β coefficient depending on the total number of cells, as well as the length of the domain. This represents an advantage since it is possible to control the size of the mesh close to the wall where the boundary layer develops. In Figure 4, an example of refinement of a 1D mesh is presented with a first cell size imposed at 10^{-2} and is compared to a more classical geometric law.

Table 1: Boundary conditions of the reference flow along the studied flat plate.

Parameters	Values
M_∞	8
p_∞	1.21114×10^4 Pa
ρ_∞	0.19475 kg.m^{-3}
T_p	1000 K

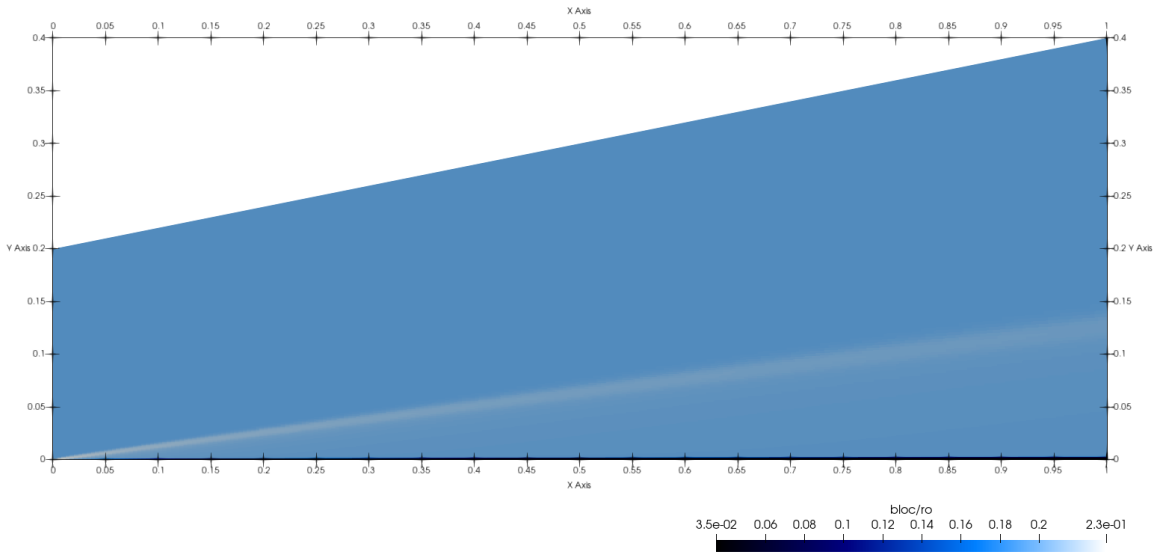

Figure 5: Density field (in kg.m^{-3}) resulting from the reference simulation of a laminar flow at $M_\infty = 8$ along a flat plate. The mesh size is 250×500, uniform in the x direction, and with a progression law in the y direction for a first mesh size of 2×10^{-8} m.

3 APPLICATION TO HYPERSONIC FLOW SIMULATIONS

3.1 Reference case of a flow along a flat plate

A reference case inspired by the work of Christopher J. Roy and Frederick G. Blottner [5] is studied. They are interested in the flow along a flat plate. The boundary conditions are recalled in the Table 1. For this test case the simulations are performed in the laminar regime. The flat plate is 1 m in size. The results of the simulation on a first mesh generated with the ICEM meshing tool were compared to those obtained with the same initial and boundary conditions on a mesh generated using our adapted mesh. In these two cases, the mesh is of size 250×500 with a uniform distribution of nodes along the x axis, and a progression law along the y axis. The size of the first cell is imposed at 2×10^{-8} m. The simulations are carried out using a Navier-Stokes calculation code based on the Roe scheme.

Figure 5 represents the solution for the density ρ in the domain after convergence on the reference mesh generated using the ICEM meshing tool. At the entrance of the domain, a very low intensity shock appears in the simulation due to the formation of a boundary layer from the leading edge at x=0.

The heat flux at the wall Φ_P plotted in Figure 6 is an indicator of the temperature gradient at the wall. The simulation results obtained on the mesh generated using ICEM and the mesh of the developed adaptation code are similar. For the two quantities presented, the curves overlap perfectly.

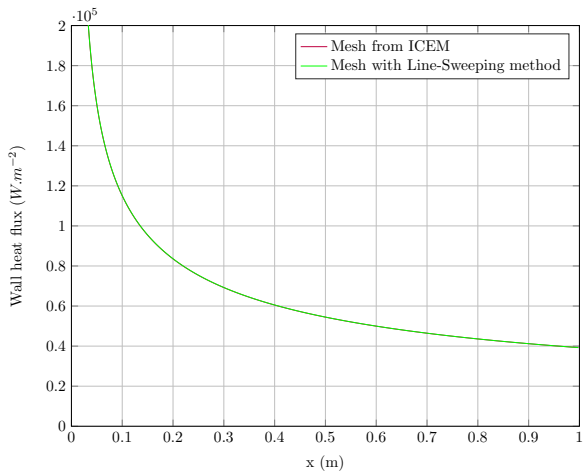

Heat flux Φ_P at the wall

Figure 6: Comparison of fluxes at the wall for the simulation of the flow with the reference mesh drawn with ICEM and a mesh of the same size (250×500) generated, randomly degraded then regularized by the Line-Sweeping method.

3.2 Case of a flow along a deformed wall

The boundary conditions are the same as the previous test case (Table 1). In this work, a deformation is applied to the wall. A Gaussian-shaped bump as presented in the article of

Prahladh S. Iyer and Mujeeb R. Malik [2] is studied. This bump is applied to the bottom edge of the mesh as follows:

$$y(x,z) = \frac{h_0}{2} e^{-(\frac{x}{x_0})^2} \tag{4}$$

where h_0 is twice the height of the bump, x_0 is a width parameter. By default, this function centers the bump around the origin of the coordinate system, so a translation must be applied to position the bump at the desired location in the domain.

The bump studied here is of height h_0=0.02 m, width x_0=0.1 m and centered at x=0.6 m as shown in Figure 7. This wall deformation is important in view of the thickness of the boundary layer and the dimensions of the problem. It was thus chosen in order to highlight the results of adaptation and regularization. On this type of configuration, the physical representation of the flow is complex.

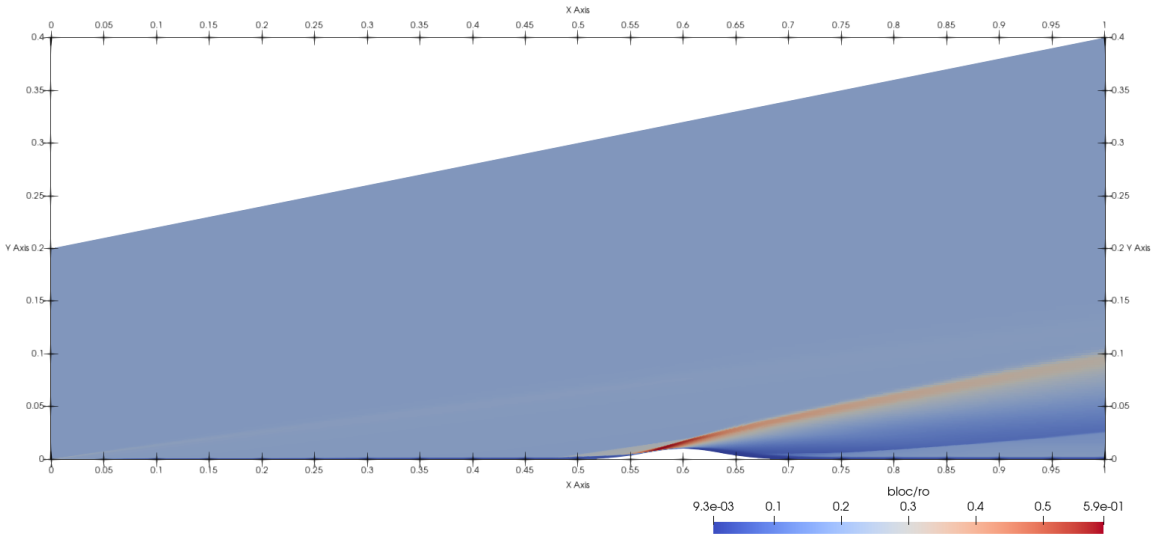

Figure 7: Density field (in kg.m^{-3}) in the field (in m) resulting from the simulation of a laminar flow at $M_\infty = 8$ around a flat plate deformed by a bump on a mesh of size 2000×500 uniform in the x direction and with a progression law in the y direction.

For the deformation studied in this part, the simulations capture macroscopically the physical phenomena as presented in Figure 7. At the entrance of the flat plate, the boundary layer develops in a manner similar to the case of the flat plate without deformation. The presence of the bump considerably modifies the flow. A shock wave appears on the bump, shown in red in Figure 7. A separation and a slight recirculation zone appear upstream of the bump (around x=0.5 m). A secondary shock wave is also observed upstream of the first separation zone. These same kind of phenomena are illustrated by Prahladh S Iyer, Suman Muppidi and Krishman

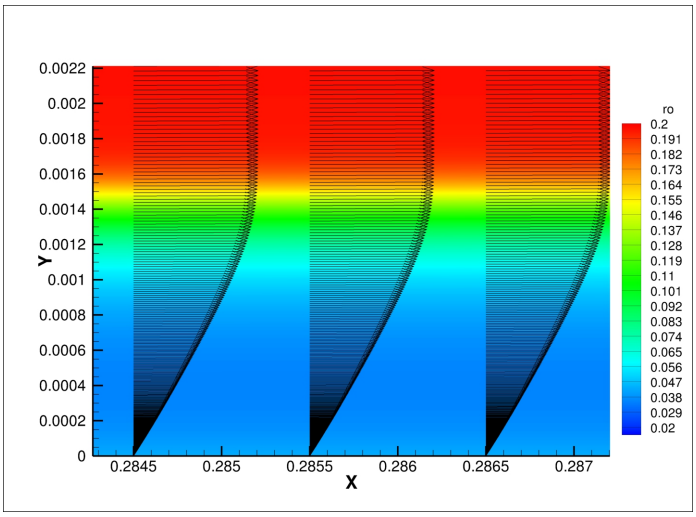

(a) Velocity profiles in the boundary layer upstream of the bump.

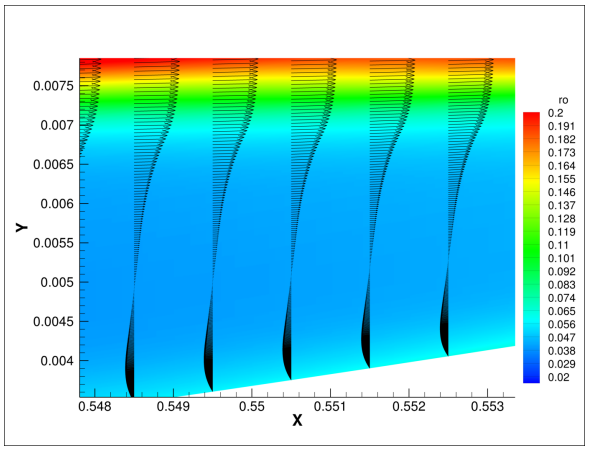

(b) Boundary layer separation zone upstream of the bump.

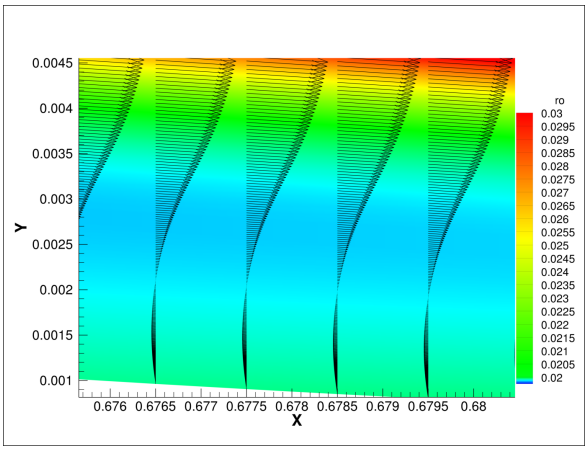

(c) Recirculation zone downstream of the bump.

Figure 8: Final near-wall fluid velocity profiles at different positions of the flat plate.

Mahesh [3] [4]. Moreover, their work seems to show that the hypothesis of considering the flow around this bump in the laminar regime at $M_\infty = 8$ is consistent.

Velocity profiles are highlighted in Figure 8 at different positions in the domain, with the density field shown in the background. The linear shape of the velocity profiles in Figure 8.(a) highlights the laminar flow regime. This zone is representative of the upstream part of the flat plate. In Figure 8.(b), a separation and recirculation zone is visible upstream of the bump due to speed cancellation. The same phenomenon appears downstream of the bump as highlighted in Figure 8.(c).

In order to study mesh convergence, the number of meshes is fixed at 1000 in the x direction. The refinement is performed in the y direction, a progression in β is applied such that the first cell is always imposed at 2×10^{-8} m. The first 4 curves in Figure 9 represent the heat fluxes at

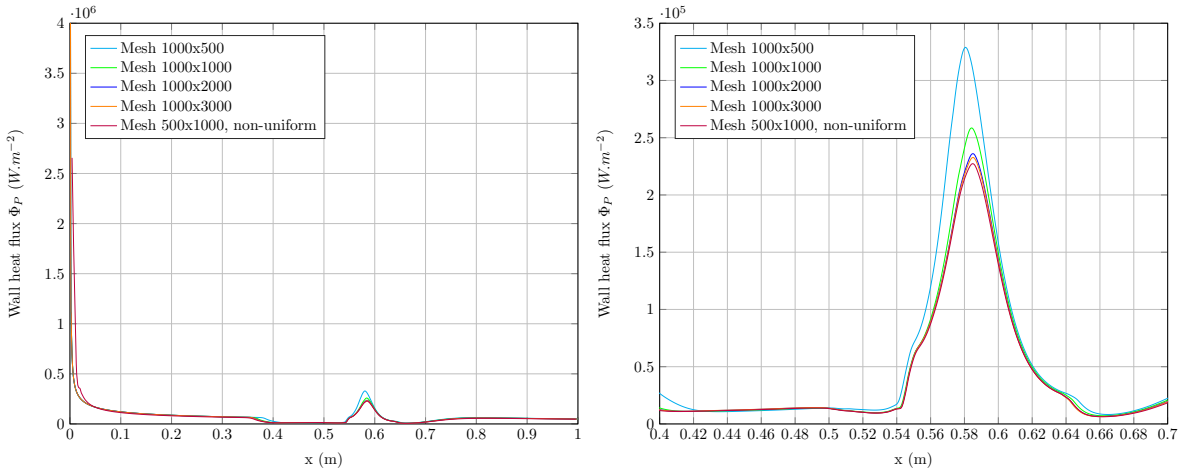

(a) Heat flux at the wall Φ_P (b) Zoom of heat flux at the wall Φ_P

Figure 9: Study of convergence on heat fluxes at the wall Φ_P. For the first 4 meshes, 1000 cells are placed evenly in the x direction whereas the last mesh is not uniform in the x direction.

the wall obtained on different meshes. A trend is clearly emerging. These meshes are composed of 300 cells each in the area of the bump ($x \in [0.45, 0.75]$) along the x axis. The non-uniform case plotted in Figure 9 was obtained with a mesh 500×1000. For this mesh, a refinement along the x axis is operated in order to place 300 cells in the zone of the bump, as for the uniform meshes. This mesh has 6 times fewer cells than the mesh of size 1000×3000 and allows capturing the same solution. These results highlight the importance of refinement work in both directions.

Table 2: Boundary conditions of the reference flow along the CCF geometry.

Parameters	Values
M_∞	6
Re_∞	5.57 10^6
p_∞	164.0 Pa
ρ_∞	0.02175 kg.m^{-3}
T_p	300 K

3.3 Case of a Cone/Cylinder/Flare geometry

We are now interested in the case of a Cone/Cylinder/Flare geometry (CCF) as in [1]. The shape of this object has been designed for wind tunnel experiments to study hypersonic boundary layer. The boundary conditions are given in the Table 2. When we apply our regularization method to the mesh the effect of our method is really visible on the nose of the CCF geometry as seen in Figure 10. On the initial mesh obtain from ICEM meshing tool we can clearly see in Figure 10.(a) the straight line on the mesh due to the blocking technique. After regularization in Figure 10.(b) the mesh is smooth and orthogonal to the wall. In Figure 11 we present the pressure around the CCF geometry. In Figure 11.(a) we can see the shock at the top of the nose whereas in Figure 11.(b) we present the shock wave around the global geometry. The main

advantage of our method is the control of the size of the first cell. In Figure 12 we present the skin friction coefficient on the CCF geometry for different size of the first cell. It is clear that if the size of the first cell is to large (here $1 \times 10^{-4} m$) we can not capture the correct solution. On the other side if the size is too small we get good solution but the number of iterations to converge increases dramatically (8000 instead of 1500 for smaller size of first cell).

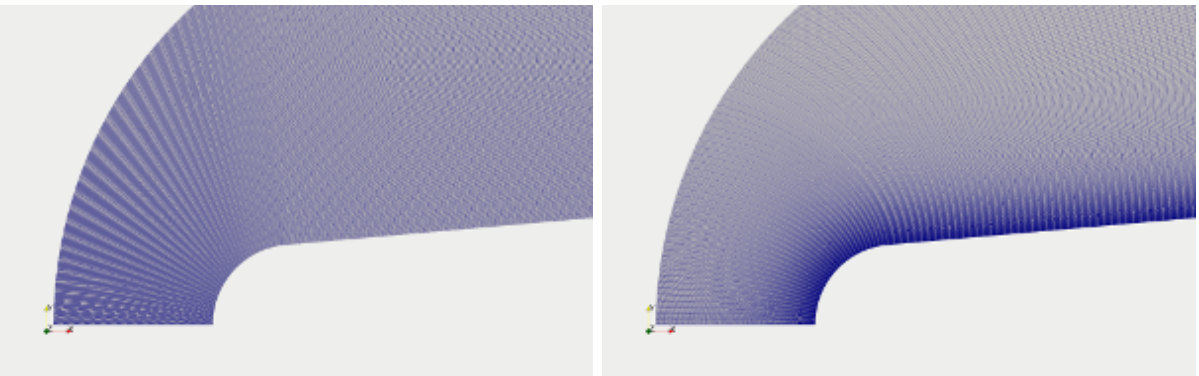

(a) Initial mesh from ICEM (a) Mesh after regularization

Figure 10: Zoom on the nose of the geometry.

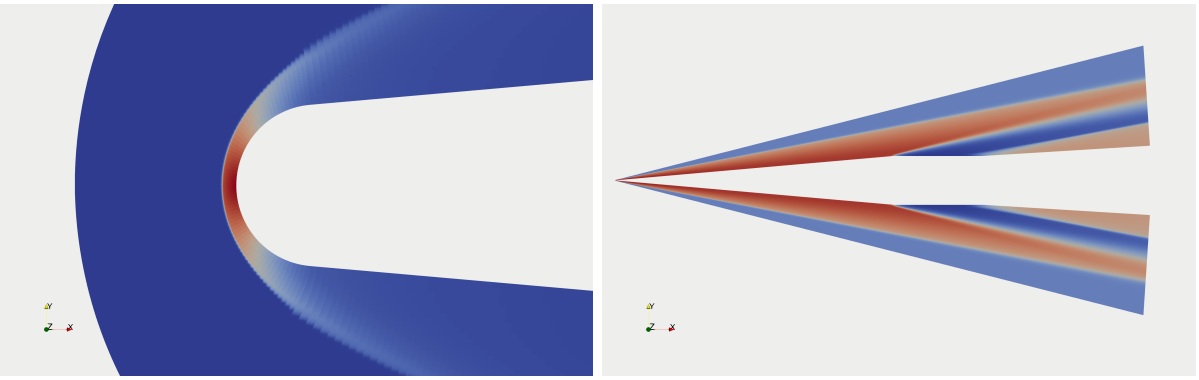

(a) Zoom on the nose (b) Shock around the geometry

Figure 11: Pressure around CCF.

4 CONCLUSION

The objective of this work was to take into account the wall deformations due to the phenomenon of ablation during the simulation of aerodynamic flows around a vehicle in atmospheric reentry in hypersonic regime. These deformations have been described directly by the deformation of the mesh. The mesh must be refined on the wall to capture the physics of the boundary layer which represents a zone of strong gradients. In addition, an orthogonalization of the mesh near the wall is necessary in order to align the meshes with the flow.

In a first part,The Line-Sweeping method introduced by J. Yao was implemented. Then the Line-Sweeping method has been adapted in order to obtain a controlled orthogonalization of the cells near the wall. Finally, a β law is applied to refine the mesh in the areas of interest in order to capture the boundary layer as well as to discretize the wall deformations. In a

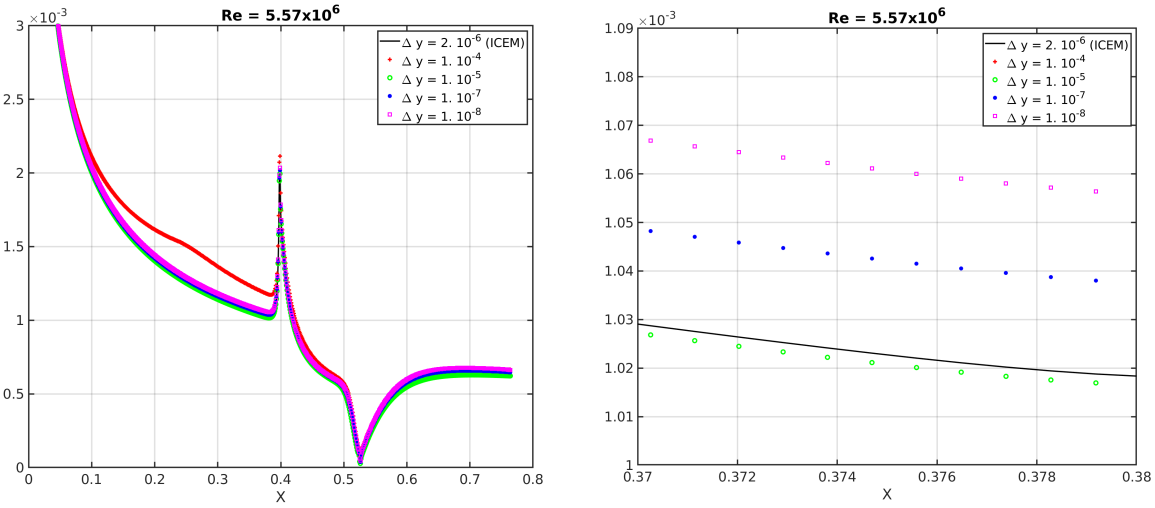

(a) Skin friction coefficient on the wall of CCF (b) Zoom on the skin friction coefficient

Figure 12: Skin friction coefficient.

last part, the developed method was applied in order to generate meshes for the simulation of flows with a Navier-Stokes CFD code. First, simulation of a flow along a deformed flat plate was studied and convergence study was performed. Finally, we also succeed in applying this regularization technique to a CCF geometry. The Line-Sweeping method can be easily extended to 3D geometries in the case of 3D structured meshes.

REFERENCES

[1] Esquieu, S. Benitez, E. Schneider, S. P. and Brazier, J.-Ph. *Flow and Stability Analysis of a Hypersonic Boundary Layer over an Axisymmetric Cone Cylinder Flare Configuration* AIAA, (2019).

[2] Prahladh, S. I. and Mujeeb, R. M. *Wall-modeled LES of flow over a Gaussian bump.* AIAA Scitech 2021 Forum, (2021).

[3] Prahladh, S. I. Suman, M. and Krishman, M. *Transition of hypersonic flow past flat plate with roughness elements.* Fluid Dynamics Conference and Exhibit, (2010).

[4] Prahladh, S. I. Suman, M. and Krishman, M. *Boundary layer transition in high-speed flows due to roughness.* AIAA 2012-1106, (2012).

[5] Roy, J. C. and Blottner, F. G. *Methodology for Turbulence Model Validation: Application to Hypersonic Flows.* Journal of Spacecraft and Rockets, 313-325, 40, (2003).

[6] Yao, J. *A Mesh Relaxation Study and Other Topics*, LLNL-TR-637101, (2013).

[7] Yao, J. *An Efficient Line-Sweep Mesh Relaxation Method with Locally Conservative Interface Reconstruction.* Lawrence Livermore National Laboratory, (2011).